REVISTA MATÉRIA V.29 N.1
ISSN 1517-7076 articles e20230173, 2024

FE simulation of uniaxial tensile behavior of SiC reinforced AA5083 alloy

Hemanth Kumar Songa[1], Koka Naga Sai Suman[2], Anjani Raj Manyala[1]

[1]GITAM (Deemed to be University), Department of Mechanical Engineering. 530045, Visakhapatnam, India.
[2]Andhra University, Department of Mechanical Engineering. 530003, Visakhapatnam, India.
e-mail: hsonga@gitam.edu, dr.knssuman@andhrauniversity.edu.in, amanyala@gitam.edu

ABSTRACT

Reinforcements added to pure AA5083 alloy are known to lower the overall weight while improving the strength of the Metal Matrix Composite (MMC). In this work, Silicon carbide (SiC) particles are added to pure AA5083 in varying quantities (3%, 5%, 7% and 10%), and tested to failure using tensile testing. The stress-strain behavior is decomposed into the elastic and plastic behavior and is validated using Finite Element (FE) modeling. The results exhibited an increase in ultimate tensile strength (UTS) of the MMC up to 5% of SiC. The formation of intermetallic compounds due to reactions at high concentrations of SiC resulted in debonding in the MMC and thus reduction in UTS. In this work, the response of the material between yield and complete failure is characterized using VOCE nonlinear model in FE analysis. It is observed that MMC with 5% SiC has shown maximum UTS (340.34 Mpa), while MMC with 10% SiC content has resulted in the most ductility (27% plastic strain) of all the compositions. Further, MMC with 7% SiC has highest saturation stress (R_0 = 653.09 Mpa) and lowest ductility, while MMC with 10% SiC has lowest saturation stress (R_0 = 115.57 Mpa) and highest ductility.

Keywords: VOCE; AA5083; Plasticity; ANSYS; Metal Matrix Composites.

1. INTRODUCTION

The addition of micro and nano reinforcement particles to a metal matrix has shown to have improved the mechanical as well as tribological properties of metal matrix composites (MMCs) [1]. Such materials with superior strength and lower weight are highly coveted in both the commutable automobile sector as well as military grade vehicles [2, 3]. Several studies focused on the addition of a wide range of reinforcements to metal matrices. SINGH *et al.* [4] showed that the addition of SiC particles in Aluminum MMCs has improved the tensile strength but reduced the elongation (or ductility) of the samples. However, the grade of Aluminum matrix and the manufacturing process (whether the sample is stir casted, friction welded or cut from a commercial rolled sample) is not mentioned. It is only logical to compare the pure sample prepared using the same method and in the same conditions as all the other samples. NAGARAJA *et al.* [5] performed a comprehensive study on the addition of Fly Ash and SiC in AA5083 and determined that the mechanical properties are mainly dependent on the sample preparation process. Usually, the reinforcements are of extremely high strength and most studies add them in powder form to the metal matrices. PIERS NEWBERY *et al.* [3] showed that ball milling at cryogenic temperatures created ultrafine grained structure which improved strength by 50% and tensile elongation by 11%. However, most studies have concentrated on the tribological properties rather than pure mechanical response. GARGATTE *et al.* [6] used liquid stir casting method to add SiC particles to Al-5083 and showed that the reinforcements reduce the wear rate when compared to pure alloy. The same has been corroborated by SOLEYMANI *et al.* [7] not just with SiC, but also with MoS_2 reinforcements. SHYAM KUMAR *et al.* [8] also used friction stir casting to develop Tungsten reinforced AA5083 alloy and proposed that a composite layer on the surface of the MMCs significantly improved the wear properties without affecting the bulk properties. TAZARI and SIADATI [9] used cold pressing and sintering for adding SiC nanoparticles to AA5083 and reported impeded grain growth

Corresponding Author: Anjani Raj Manyala Received on 08/06/2023 Accepted on 15/01/2024

DOI: https://doi.org/10.1590/1517-7076-RMAT-2023-0173

being the reason for improved strength and wear properties of reinforced MMCs. FOO *et al.* [10] in an early study found out that at high temperatures during sintering, intermetallic compounds may be created at the SiC-matrix interface, though not in all the cases. These compounds had caused debonding at the interface and can reduce the strength. ALIZADEH *et al.* [11] proposed that a combined stir casting and squeeze casting technique significantly improved particle distribution which resulted in improved strength and wear properties. JAIN *et al.* [12] demonstrated that Zener-Holloman mechanism and particle stimulated nucleation (PSN) mechanism has been activated during friction stir casting of SiC into AA5083 which resulted in randomly oriented grains. GHOSH and SAHA [13] showed that the crack density increases with increase in SiC (direct metal laser sintered) volume beyond 15% and wear resistance reduces beyond 20% volume. When it comes to determining the mechanical response of the reinforced MMCs using FE models, several approaches are being used. Representative or unit volume element approach wherein one single cell with the volume fraction of the reinforcement embedded into the matrix has been the most common form of modeling reinforced composites in finite element modeling [14]. More advanced techniques such as modeling of the exact shape and volume of the reinforcement into a finite volume has also been done [15]. However, the bonding of the elements is not a precise science, and it would be computationally expensive to model a macro specimen. BALASIVANANDHA PRABU *et al.* [16] studied the interface between the Al matrix and the SiC microparticles at a microscopic scale and concluded that apart from the size of the particles, their orientation also affects the overall response. PENG *et al.* [17] has performed a comprehensive 3D multiscale analysis of micro and nano-reinforcements in MMCs. They created Representative Volume Elements (RVEs) to model macroscale responses using FE analysis and estimated progressive damage and fracture. A similar study was done by SAXENA *et al.* [18] on reinforcements to Copper MMCs. BAHL and BAGHA [19] used 2D FE analysis to study the interfacial effects between the reinforcements and the metal matrix and reported that the cohesive layer behaved the same as the matrix before damage. KIM *et al.* [20] analyzed various interface techniques and microstructure analyses to study their effect on the material properties of the MMCs. MAURYA *et al.* [21] reviewed the reinforcements that are usually added to the Aluminum MMCs.

PALANIYANDI and VEEMAN [22] indicated the extraordinary performance of Aluminium MMCs was the low density that obtained after alloying. Ultimate tensile strength, compressive strength and impact toughness improves with the addition of reinforced particle. GOVINDAN and RAGHUVARAN [23] stated that when the weight % of reinforcement rises, the elastic strength increases gradually, and toughness will be limited resulting in an increase in matrix rigidity. S. IYENGAR et al. [24] reviewed that the increased tensile strength is attributed to good dispersion and interfacial bonding between the particles and Aluminium metal matrix. WOLF et al. [25] inferred the mechanical strength of the composites were superior to the matrix material, especially for the aluminum alloy composites which showed significant increase on the UTS. NANJAN and MURALI [26] has observed the enhancement of mechanical properties of the stir casted metal matrix composites. BARMOUZ et al. [27] has discovered the formation of the intermetallic phases between the base metal and reinforced particles in the casted specimens. CAO et al. [28] has discovered that the behavior of the reinforced particles changes with the processing parameters. GUKENDRAN et al. [29] concluded that the introduction of reinforcements into aluminium enhances the mechanical properties of the composites considerably.

In this work, the stress-strain curves of the SiC reinforced AA5083 prepared by stir-casting method are analyzed to characterize the material response in both the elastic and plastic regime with emphasis on the plasticity behavior. Influence of the SiC particles on the strength and ductility of the MMCs is studied and the FE parameters that influence the response of the MMCs in the nonlinear regime are identified.

2. MATERIALS AND METHODS

The sample was prepared as per ASTM E8/E8M – 13a [30] as shown in Figure 1. The subsize specimen which is the smallest of all the 3 specified sizes was chosen (to minimize material usage). The steps involved in sample preparation and the microstructure analysis of the specimens is already documented in a previously published work [31].

The experimental procedure is as follows. The sample is placed in the grips exactly for 20 mm from both ends and was loaded at a rate of 1 mm/min until failure. A servo hydraulic 100 kN INSTRON 8801 universal testing machine is used for experimentation. 5 different types of specimens are tested. Apart from the pure AA5083 specimen, samples made with the addition of 3%, 5%, 7% and 10% SiC to pure AA5083 are tested. Every aspect of the experiment is carefully documented to replicate the process in using FE Analysis. The specimens exhibited classic brittle failure with little to no necking as shown in Figure 2. However, based on the final length of the specimens, a significant elongation can be observed though no

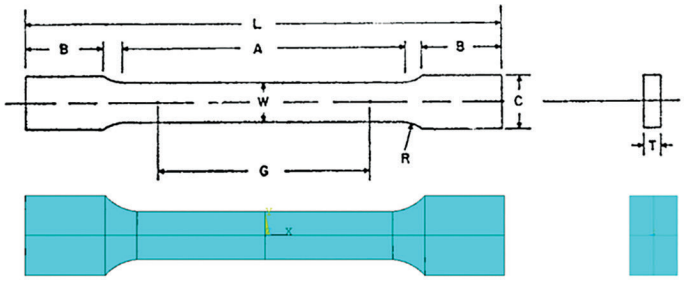

Dimensions	mm
G – Gauge Length	25
W - Width	6
T - Thickness	6
R – Fillet Radius	6
L – Overall Length	100
A – Length of reduced section	32
B – Length of grip section	30
C – Width of grip section	10

Figure 1: ASTM standards for tensile testing [30].

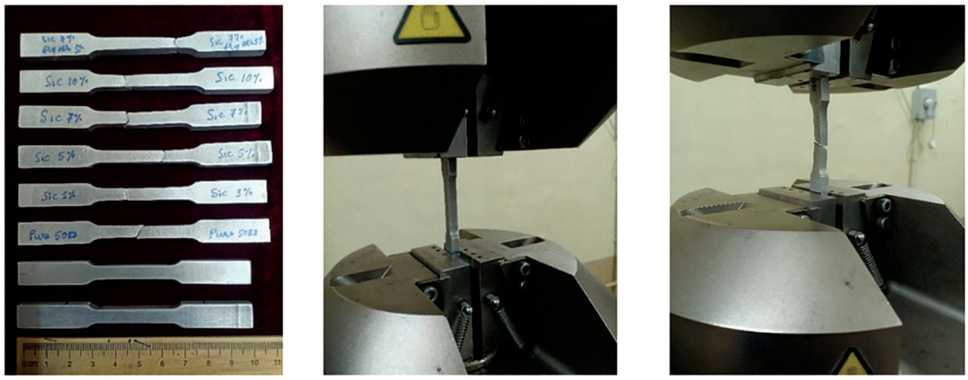

(a) (b) (c)

Figure 2: (a) Prepared and tested samples (b) sample before testing (c) sample after testing.

Table 1: Experimental data.

COMPOSITE	ELASTIC MODULUS (Mpa)	EXPERIMENTAL	
		TENSILE STRESS AT YIELD (0.2% OFFSET) (Mpa)	ULTIMATE TENSILE STRESS (Mpa)
Pure AA5083	56302	117.78	238.31
AA5083 + 3% SiC	66999	127.35	256.61
AA5083 + 5% SiC	64165	127.68	263.73
AA5083 + 7% SiC	67699	129.53	254.37
AA5083 + 10% SiC	60504	118.98	243.75

necking has occurred. The complete stress strain curves of the tests are published in KUMAR *et al.* [31]. Once the experimental data is obtained, further analysis is performed as explained in the subsequent sections.

3. RESULTS AND DISCUSSION

3.1. Experimental results

The results obtained from the UTM (INSTRON) are shown in Table 1. These parameters are based on the Engineering Stress-Strain data calculated using the initial length and cross-section area of the samples.

Figure 3 shows the stress strain data of the pure AA5083 sample obtained the INSTRON UTM. The linear region of the stress-strain data is not exactly clear from the curve and needs closer examination (Figure 4) to identify the linear and non-linear regions.

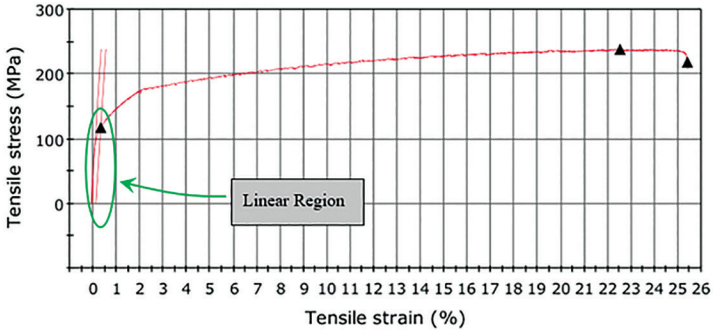

Figure 3: Stress-strain curve of the Pure AA5083 sample.

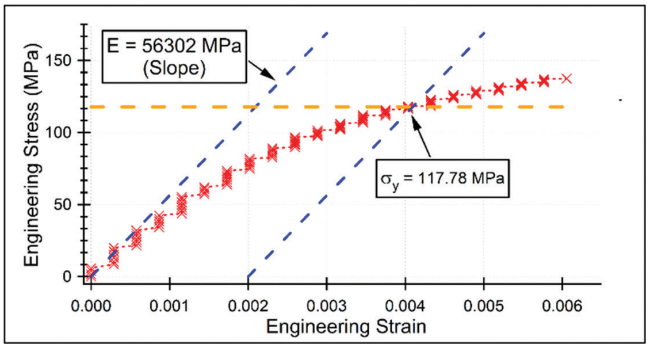

Figure 4: Close-up of the linear region of the stress strain curve of Pure AA5083 sample.

3.2. Plasticity analysis

The major objective of this work is to analyze the plastic region of the stress-strain curve. Hence, it is first required to separate the data into elastic and plastic regions. The decomposition of the experimental stress-strain data into elastic and plastic regions is a challenging task since the identification of the linear region of the stress-strain curve is not an exact science. One has to make a decision on how much non-linearity is acceptable in the elastic portion of the curve. The "Elastic Modulus" and "Tensile stress at yield (0.2% offset)" data obtained from INSTRON (Table 1) is taken as reference.

However, analysis of the linear elastic region is not the intent of this paper. This paper considers the yield point (Tensile Stress at Yield (0.2% Offset) obtained from the instrument as the starting point for further analysis. As such, the procedure adopted here to separate the elastic and plastic regions is as follows:

$$\varepsilon_p = \varepsilon_t - \varepsilon_E = \varepsilon_t - \sigma / E \tag{1}$$

where $\varepsilon_p, \varepsilon_t, \varepsilon_E, \sigma, E$ are true plastic strain, true total strain, true elastic strain, true stress and Young's modulus respectively [32]. Since the experimentation only involves uniaxial tests, the equivalent stress and strain are the same as the total stress and strain [33]. For multiaxial loads, the calculations involve lot more complexity. For finding out true stress strain values, the experimental stress-strain data (also called engineering stress-strain or nominal stress-strain) is converted as follows:

The true strain ε is calculated from engineering strain 'e' as follows:

$$\varepsilon = ln(e+1) \tag{2}$$

The true stress σ is obtained from engineering stress, 's' as follows:

$$\sigma = \frac{P}{A_0}(e+1) = s(e+1) \tag{3}$$

The tensile stress at yield point (σ_0) obtained from experimental data is shown in Table 1 is taken as the reference for the onset of yielding. The strain at that point (maximum true elastic strain) is subtracted from the subsequent true strain value so that only the plastic strain values are remaining. The true stress

Table 2: True stress values of yield and ultimate tensile strength values.

COMPOSITE	TRUE	
	TENSILE STRESS AT YIELD (0.2% OFFSET) (Mpa)	ULTIMATE TENSILE STRESS (Mpa)
Pure AA5083	119.08	296.22
AA5083 + 3% SiC	128.67	306.17
AA5083 + 5% SiC	129.12	340.34
AA5083 + 7% SiC	130.94	293.24
AA5083 + 10% SiC	120.39	317.26

values thus obtained are listed in Table 2. In this work, rather than making observations with this data, a nonlinear plasticity model is used to fit the data up until the failure point. It has to be noted here that the plasticity model can only predict the path of the stress-strain curve and not the breaking stress. The breaking stress usually depends on the imperfections in the samples which are not taken into consideration in the theoretical model.

Based on these numbers, the results of the Pure AA5083 are taken for reasoning. Figure 3 shows the entire stress strain curve of the sample and Figure 4 shows the close up of the elastic region of the curve. It can be clearly seen that the slope (56302 MPa) as interpreted by the inbuilt software does not accurately fit the data.

3.3. Analytical parameter identification

The VOCE model mainly used to capture work hardening characterizes yield stress in the material using an exponential saturation term in addition to a linear term as shown in Eqn (4) below:

$$\sigma_Y = \sigma_0 + R_0\hat{\varepsilon}^{pl} + R_\infty(1 - exp(-b\hat{\varepsilon}^{pl})) \tag{4}$$

where the user-defined parameters R_∞, the difference between the saturation stress and the initial yield stress, R_0, the slope of the saturation stress and, b, the hardening parameter that governs the rate of saturation of the exponential term $\hat{\varepsilon}^{pl}$ is the accumulated equivalent plastic strain. Eqn (4) shows the progression of yield stress beyond the initial yield stress σ_0. To apply this model, the plastic strain $(\hat{\varepsilon}^{pl})$ is to be separated from the total strain and the initial yield stress (σ_0) must be identified from the experimental data. MASTRONE *et al.* [34] followed an iterative procedure to obtain the Voce parameters for a ductile material. In this work, the initial yield stress is constrained to be the same as obtained from the experiment and the rest of the parameters are optimized using a Generalized Reduced Gradient (GRG) nonlinear method without any constraints.

The curve fits to the actual true plastic stress to equivalent plastic stress are as shown in Figure 5 and Table 3. The figure clearly shows the higher stress response for certain MMCs over others. Another inference that can be made from Figure 5 is the amount of equivalent plastic strain. Assuming that the elastic strain can be re-covered, the amount of equivalent plastic strain is considered as the ductility of the material. The maximum ductility can thus be seen for 10% SiC added MMC with a value of 0.27 or 27% followed by 5% SiC added MMC with 25%.

The plot of these parameters along with the Elastic Modulus (E) has been shown in Figure 6. The following observations are made from these plots: The elastic modulus (E) and σ_0 follow a similar trend and higher for MMCs compared to the pure AA5083, but a clear drop can be observed at 10% SiC. The R_0 and b values which show a similar trend, shows that the highest slope of the saturation stress or the fastest rise after yield point is observed in the 7% SiC MMC. The R_∞ values which represent the ductility or the longest strain between the saturation (break) and yield is highest for the 10% SiC which had an equivalent plastic strain of close to 27% before break. Though the exact reason of the break can only be ascertained using microscopic analysis, the most likely reason is the sudden debonding of the interfacial layer due to high slopes of the stress.

3.4. Finite element analysis

ANSYS 15.0 Academic version is used for the analytical evaluation of the material response. The 1/8th symmetric model of the specimen is modeled as shown in Figure 7. The dimensions of this model are given in Figure 1. The details of the element type used, and material properties are shown in Table 4.

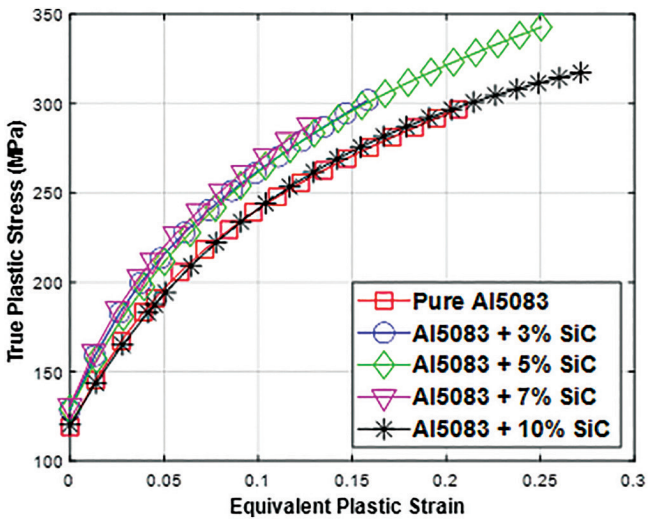

Figure 5: GRG curve fits of all the materials used.

Table 3: The VOCE parameters obtained by fitting the experimental data with Eqn (4) using the GRG method.

	PURE AA5083	AA5083 +3% SiC	AA5083 +5% SiC	AA5083 +7% SiC	AA5083 +10% SiC
σ_0	119.0838	128.6714	129.1231	130.9448	120.3919
R_0	361.6365	579.7463	329.3432	653.0933	115.5742
R_∞	106.7094	83.3625	136.1315	76.6707	179.6840
b	16.2338	23.8436	13.2070	26.7469	9.3645

The model is built as 4 volumes to control the mesh size and also for application of boundary conditions. The left most volume and the adjacent filleted volume of the model are fine meshed, whereas the right most volume is coarse meshed. The coarse meshed volume is the region that is fixed inside the grips of the vice during experimentation. The mesh is shown in Figure 8. The total number of brick elements is 4920 and the total number of nodes is 23773.

3.5. Boundary conditions

Since the model is 1/8th symmetric, the 3 faces of the model (i.e. areas along xy = 0, yz = 0 and xz = 0) are constrained with symmetric boundary conditions as shown in Figure 9(a). The symmetry conditions imply that the surfaces cannot move along their normal. All the nodes within the grips are coupled in the direction of motion so that they move together. For loading, the load applied can be either displacement controlled or load controlled. The choice of load control greatly affects the convergence of the solution. However, that description is beyond the scope of this paper. Here, the optimum convergence occurs with force control where the actual force (obtained from experiment) is distributed uniformly on all the nodes that are constrained in the grips (Figure 9(b)). The load is applied in steps using auto time stepping. Since the material model chosen is rate independent, the rate at which the load is applied does affect the solution.

The stress plot (in the x-direction) for the pure AA5083 sample is shown in Figure 10(a) where the maximum stress is expected to occur because of the minimum amount of cross-section. The stress-strain plot at the global origin i.e. the middle of the fill specimen is taken for evaluating the stress and strain data as shown in Figure 10(b).

The stress-strain curves obtained using FE analysis is compared with the experimental data and the fit is shown in Figure 11. The plot shows only the fit of best composition of MMC (AA5083 + 5% SiC) and the pure AA5083 alloy. The FE result closely matched the experimental results in all the categories, but due to cluttering of the data, only 2 sets of data is presented here. Hence, this process of material property extraction for FE analysis can be used for MMCs.

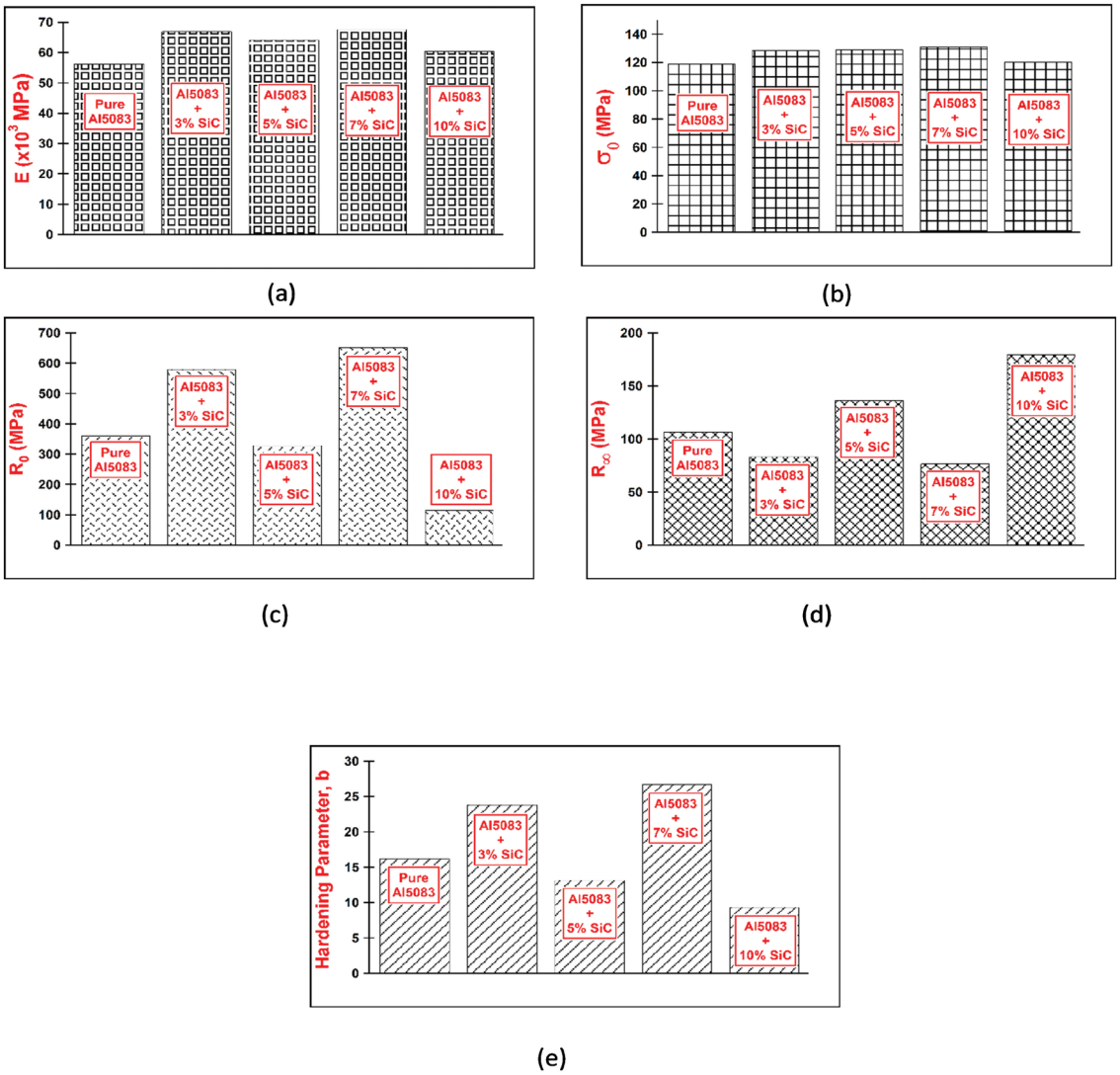

Figure 6: The variation of (a) elastic modulus, E (b) initial yield stress, σ_0 (c) slope of the saturation stress, R_0 (d) difference between the saturation stress and the initial yield stress, R_∞ (e) hardening parameter, b.

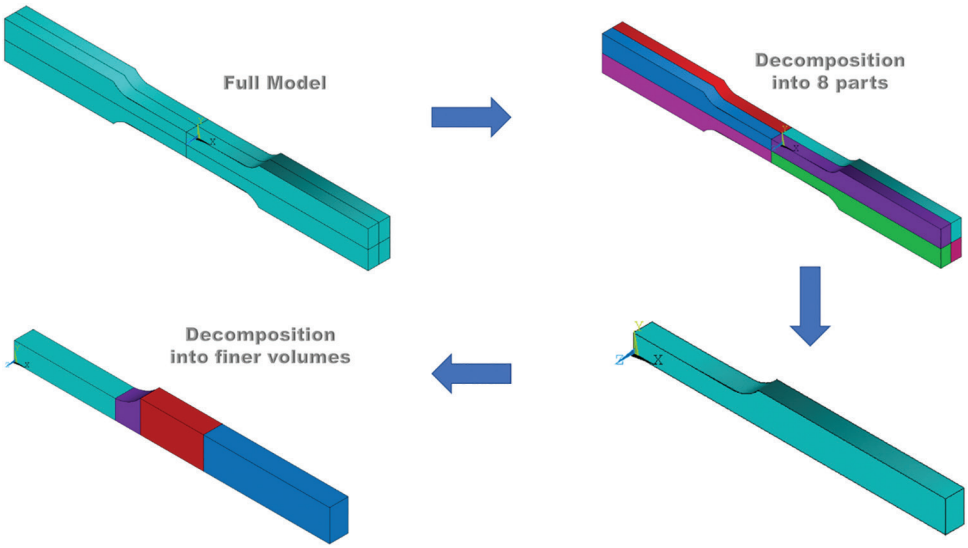

Figure 7: Modeling of 1/8th symmetric model from the full tensile testing specimen.

Table 4: Element type and material models used in FEA.

ELEMENT TYPE	MATERIAL MODEL (REQUIRED PARAMETERS)
SOLID186 (20-node bricks)	*Nonlinear inelastic rate independent isotropic hardening Mises plasticity model*
	Elastic Modulus: (Table 1) Poisson's ratio: 0.3 Initial Yield Stress, σ_0 (Table 3) Linear Coefficient, R_0 (Table 3) Exponential Coefficient, R_∞ (Table 3) Exponential Saturation Parameter, b (Table 3)

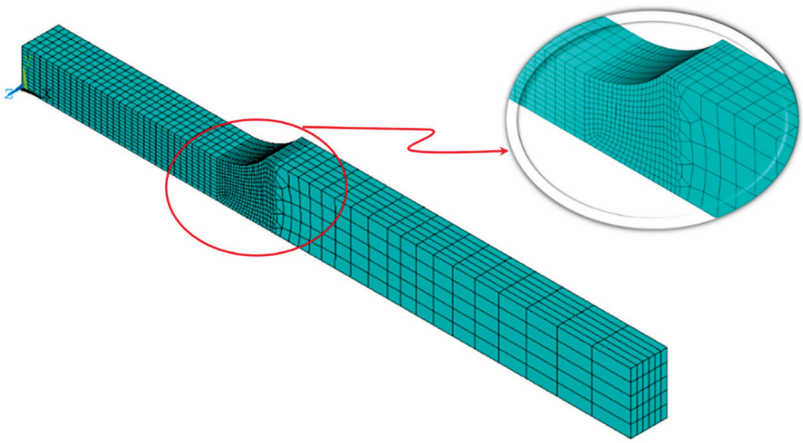

Figure 8: Mesh of the FEA model.

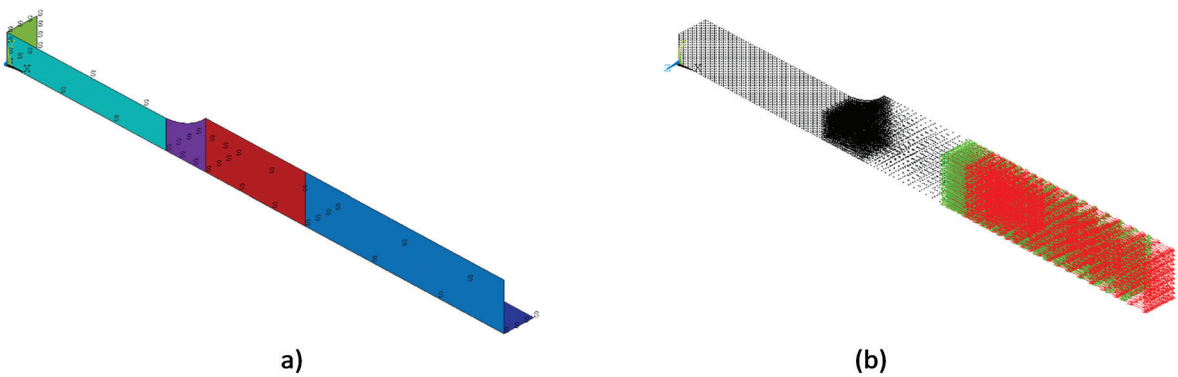

Figure 9: (a) Symmetry boundary conditions on the areas (b) force applied on the coupled nodes in the x-direction.

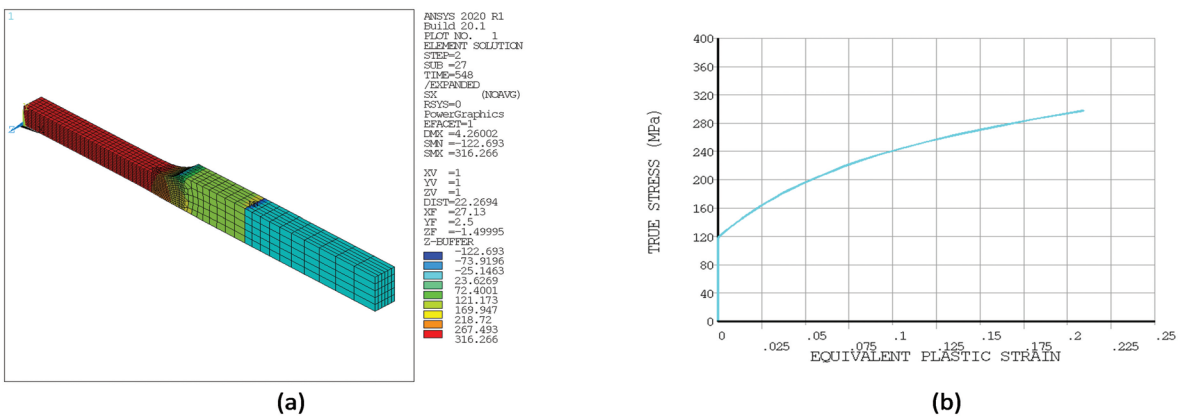

Figure 10: (a) Axial stress plot at maximum deformation and (b) the stress strain curve on the smallest section.

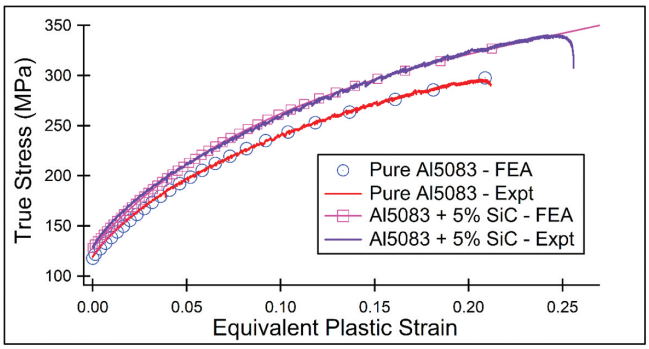

Figure 11: The stress strain curves obtained from FEA in comparison to experimental data.

4. CONCLUSIONS

The algorithm performed by the commercial software inbuilt in the equipment for interpretation of experimental data depends on the regression algorithm used and manual interpretation of data need to be performed as per the standard procedure. This can be seen from the calculation of Young's modulus and Initial Yield Stress values as seen in Figure 4.

Though the mode of failure appears to be brittle and no necking can be seen, there is significant amount of elongation in the MMCs before failure (27% for 10% addition of SiC).

Even though, ductility is significant, the material failure shows a brittle characteristic rather than classical ductile failure. The brittle fracture is because of the manufacturing process involved in preparing the samples. A rolled sample will exhibit classic ductile fracture but a cast specimen as in this case will have imperfections which will lead to sudden crack formation and propagation which leads to brittle failure.

Addition of Silicon carbide (SiC) particles to pure AA5083 in varying quantities (3%, 5%, 7% and 10%) has resulted in increased ultimate tensile strength (UTS) of the MMC upto to 5% SiC, but as the SiC content increased further, the strength has deceased. This result can be attributed to the formation of intermetallic particles that seem to have formed due to reactions at high concentrations of SiC.

When it comes to final failure, a clear trend has not been observed. However, the 10% SiC MMC has shown the most equivalent plastic strain (27%) which is a measure of ductility.

The highest slope of the saturation stress or the fastest rise after Yield point is observed in the 7% SiC MMC. It is also the MMC with the least amount of plastic strain before failure.

Looking at the overall result, the MMC with 5% SiC has the optimum combination of ductility and ultimate tensile strength.

Finally, the results have shown that the plastic material properties extracted with the process described here are adequate for Finite Element Analysis of materials in the nonlinear domain.

5. ACKNOWLEDGMENTS

The authors thank Dr. Rajeswara Resapu, Associate Professor, Department of Mechanical Engineering, GITAM (Deemed to be University) for his valuable suggestions in regards to Finite Element Modeling and Analysis.

6. BIBLIOGRAPHY

[1] PAL, B., GHOSH, S., SAHOO, P., "Aluminium Hybrid Composites Reinforced with SiC and Fly Ash Particles: Recent Developments", In: Sahoo, S. (eds), *Recent Advances in Layered Materials and Structures. Materials Horizons: From Nature to Nanomaterials. Springer, Singapore.,* pp. 133–170, 2021. doi: http://dx.doi.org/10.1007/978-981-33-4550-8_6.

[2] CHANDEL, R., SHARMA, N., BANSAL, S.A., "A review on recent developments of aluminum-based hybrid composites for automotive applications", *Emergent Materials,* v. 4, n. 5, pp. 1243–1257, 2021. doi: http://dx.doi.org/10.1007/s42247-021-00186-6.

[3] PIERS NEWBERY, A., NUTT, S.R., LAVERNIA, E.J., "Multi-scale Al 5083 for military vehicles with improved performance", *Journal of the Minerals Metals & Materials Society*, v. 58, n. 4, pp. 56–61, 2006. doi: http://dx.doi.org/10.1007/s11837-006-0216-4.

[4] SINGH, V., CHAUHAN, S., GOPE, P., *et al.,* "Enhancement of wettability of aluminum based silicon carbide reinforced particulate metal matrix composite", *High-Temperature Materials and Processes*, v. 34, n. 2, pp. 163–170, 2014. doi: http://dx.doi.org/10.1515/htmp-2014-0043.

[5] NAGARAJA, S., KODANDAPPA, R., ANSARI, K., *et al.,* "Influence of heat treatment and reinforcements on tensile characteristics of aluminium AA 5083/silicon carbide/fly ash composites", *Materials (Basel),* v. 14, n. 18, pp. 5261, 2021. doi: http://dx.doi.org/10.3390/ma14185261. PubMed PMID: 34576489.

[6] GARGATTE, S., UPADHYE, R.R., DANDAGI, V.S., *et al.,* "Preparation & characterization of Al-5083 alloy composites", *Journal of Minerals & Materials Characterization & Engineering,* v. 1, n. 01, pp. 8–14, 2013. doi: http://dx.doi.org/10.4236/jmmce.2013.11002.

[7] SOLEYMANI, S., ABDOLLAH-ZADEH, A., ALIDOKHT, S.A., "Microstructural and tribological properties of AA5083 based surface hybrid composite produced by friction stir processing", *Wear*, v. 278–279, pp. 41–47, 2012. doi: http://dx.doi.org/10.1016/j.wear.2012.01.009.

[8] SHYAM KUMAR, C.N., BAURI, R., YADAV, D., "Wear properties of 5083 Al-W surface composite fabricated by friction stir processing", *Tribology International*, v. 101, pp. 284–290, 2016. doi: http://dx.doi.org/10.1016/j.triboint.2016.04.033.

[9] TAZARI, H., SIADATI, M.H., "Nanocomposites of AA5083/SiC, strength and wear behaviors", *Materials Research Express*, v. 6, n. 10, pp. 105084, 2019. doi: http://dx.doi.org/10.1088/2053-1591/ab3b91.

[10] FOO, K.S., BANKS, W.M., CRAVEN, A.J., *et al.,* "Interface characterization of an SiC particulate/6061 aluminium alloy composite", *Composites,* v. 25, n. 7, pp. 677–683, 1994. doi: http://dx.doi.org/10.1016/0010-4361(94)90201-1.

[11] ALIZADEH, A., KHAYAMI, A., KARAMOUZ, M., *et al.,* "Mechanical properties and wear behavior of AA5083 matrix composites reinforced with high amounts of SiC particles fabricated by combined stir casting and squeeze casting, a comparative study", *Ceramics International*, v. 48, n. 1, pp. 179–189, 2022. doi: http://dx.doi.org/10.1016/j.ceramint.2021.09.093.

[12] JAIN, V.K.S., YAZAR, K.U., MUTHUKUMARAN, S., "Development and characterization of AA5083-CNTs/SiC composites via friction stir processing", *Journal of Alloys and Compounds*, v. 798, pp. 82–92, 2019. doi: http://dx.doi.org/10.1016/j.jallcom.2019.05.232.

[13] GHOSH, S.K., SAHA, P., "Crack and wear behavior of SiC particulate reinforced aluminium based metal matrix composite fabricated by direct metal laser sintering process", *Materials & Design*, v. 32, n. 1, pp. 139–145, 2011. doi: http://dx.doi.org/10.1016/j.matdes.2010.06.020.

[14] RAO, P.K.V., RAGHUKUMAR, B., VEERA SAI CHANDH, Y., *et al.,* "Finite element analysis of CNT reinforced aluminium composite subjected to mechanical loading", *Materials Today: Proceedings,* v. 16, pp. 308–313, 2019. doi: http://dx.doi.org/10.1016/j.matpr.2019.05.095.

[15] SHEN, H., LISSENDEN, C.J., "3D finite element analysis of particle-reinforced aluminum", *Materials Science and Engineering A*, v. 338, n. 1, pp. 271–281, 2002. doi: http://dx.doi.org/10.1016/S0921-5093(02)00094-1.

[16] BALASIVANANDHA PRABU, S., KARUNAMOORTHY, L., KANDASAMI, G.S., "A finite element analysis study of micromechanical interfacial characteristics of metal matrix composites", *Journal of Materials Processing Technology*, v. 153–154, pp. 992–997, 2004. doi: http://dx.doi.org/10.1016/j.jmatprotec.2004.04.157.

[17] PENG, Y., ZHAO, H., YE, J., *et al.,* "Multiscale 3D finite element analysis of aluminum matrix composites with nano&micro hybrid inclusions", *Composite Structures,* v. 288, pp. 115425, 2022. doi: http://dx.doi.org/10.1016/j.compstruct.2022.115425.

[18] SAXENA, A., DWIVEDI, S.P., MAURYA, N.K., *et al.,* "Investigation on mechanical properties and deformation behavior of copper-based three-phase metal matrix composite: experimental and micro-macro-mechanical finite element analysis", *Journal of Materials: Design and Applications*, v. 235, n. 8, pp. 1850–1867, 2021.

[19] BAHL, S., BAGHA, A.K., "Finite element modeling and simulation of the fiber-matrix interface in fiber reinforced metal matrix composites", *Materials Today: Proceedings*, v. 39, pp. 70–76, 2021. doi: http://dx.doi.org/10.1016/j.matpr.2020.06.160.

[20] KIM, D., CHANG, H.J., CHOI, H., "Microscopic analysis of metal matrix composites containing carbon Nanomaterials", *Applied Microscopy*, v. 50, n. 1, pp. 4, 2020. doi: http://dx.doi.org/10.1186/s42649-019-0024-2. PubMed PMID: 33580328.

[21] MAURYA, M., KUMAR, S., BAJPAI, V., "Assessment of the mechanical properties of aluminium metal matrix composite: A review", *Journal of Reinforced Plastics and Composites*, v. 38, n. 6, pp. 267–298, 2018. doi: http://dx.doi.org/10.1177/0731684418816379.

[22] PALANIYANDI, S., VEEMAN, D., "Experimental investigation of mechanical performance of basalt/epoxy/MWCNT/SiC reinforced hybrid fiber metal laminates.", *Materials Research*, v. 25, pp. 25, 2022. doi: http://dx.doi.org/10.1590/1980-5373-mr-2022-0174.

[23] GOVINDAN, K., RAGHUVARAN, J.G., "Mechanical properties and metallurgical characterization of LM25/ZrO_2 composites fabricated by stir casting method.", *Matéria (Rio de Janeiro)*, v. 24, n. 3, pp. e12439, 2019. doi: http://dx.doi.org/10.1590/s1517-707620190003.0753.

[24] IYENGAR, S., SETHURAM, D., SHOBHA, R., *et al.,* "Microstructure, microhardness, and tensile properties of hot-rolled Al6061/TiB2/CeO2 hybrid composites", *Journal of the Southern African Institute of Mining and Metallurgy*, v. 121, n. 10, pp. 543–548, 2021. doi: http://dx.doi.org/10.17159/2411-9717/1560/2021.

[25] WOLF, W., ALIAGA, L.C.R., TRAVESSA, D.N., *et al.,* "Enhancement of mechanical properties of aluminum and 2124 aluminum alloy by the addition of quasicrystalline phases.", *Materials Research*, v. 19, pp. 74–79, 2016. doi: http://dx.doi.org/10.1590/1980-5373-mr-2016-0088.

[26] NANJAN, S., MURALI, J.G., "Analysing the mechanical properties and corrosion phenomenon of reinforced metal matrix composite.", *Materials Research*, v. 23, n. 2, pp. 23, 2020. doi: http://dx.doi.org/10.1590/1980-5373-mr-2019-0681.

[27] BARMOUZ, M., ZALL, V., PASHAZADEH, H., "Mechanical and microstructural characterization of hybrid Cu-SiC-Zn Composites fabricated via friction stir processing.", *Materials Research*, v. 19, n. 6, pp. 19, 2016. doi: http://dx.doi.org/10.1590/1980-5373-mr-2016-0152.

[28] CAO, C., ZHANG, X., CHEN, T., *et al.,* "Effects of processing parameters on microstructure and mechanical properties of powder-thixoforged SiC p/6061 Al composite.", *Materials Research*, v. 20, n. 1, pp. 236–248, 2017. doi: http://dx.doi.org/10.1590/1980-5373-mr-2016-0466.

[29] GUKENDRAN, R., SAMBATHKUMAR, M., SASIKUMAR, K.S.K., *et al.,* "Effect of silicon carbide and alumina reinforcement of different volume fraction on wear characteristics of AL 7075 hybrid composites using response surface methodology.", *Materials Research*, v. 25, pp. 25, 2022. doi: http://dx.doi.org/10.1590/1980-5373-mr-2022-0204.

[30] ASTM standard E8/E8M:13a., *"Standard Test Methods for Tension Testing of Metallic Materials"*, ASTM International, West Conshohocken, 2019.

[31] KUMAR, S.H., SUMAN, K.N.S., SEKHAR, S.R., *et al.,* "Investigation of mechanical and tribological properties of aluminium metal matrix composites", *Materials Today: Proceedings*, v. 5, n. 11, Part 3, pp. 23743–23751, 2018. doi: http://dx.doi.org/10.1016/j.matpr.2018.10.165.

[32] SMITH, M., *ABAQUS/Standard User's Manual, Version 6.9*, Providence, RI, Dassault Systèmes Simulia Corp, 2009.

[33] BARKEY, M.E., LEE, Y., "Strain-based multiaxial fatigue analysis", In: Y. Lee, M.E. Barkey, H. Kang (eds.), *Metal Fatigue Analysis Handbook*, chapter 8, Boston, Butterworth-Heinemann, pp. 299–331, 2012. doi: http://dx.doi.org/10.1016/B978-0-12-385204-5.00008-2.

[34] MASTRONE, M., FRACCAROLI, L., CONCLI, F., "Ductile damage model of an aluminum alloy: experimental and numerical validation on a punch test", *International Journal of Computational Methods and Experimental Measurements*, v. 9, n. 3, pp. 249–260, 2021. doi: http://dx.doi.org/10.2495/CMEM-V9-N3-249-260.